Received: 14 October 2020 | Revised: 6 April 2021 | Accepted: 7 April 2021

DOI: 10.1002/esp.5135

RESEARCH ARTICLE

ESPL WILEY

Mapping potential surface ponding in agriculture using UAV-SfM

Eugenio Straffelini[1] | Sara Cucchiaro[1,2] | Paolo Tarolli[1]

[1]Department of Land, Environment, Agriculture and Forestry, University of Padua, Agripolis, Viale dell'Università 16, Legnaro (PD), 35020, Italy

[2]Department of Agricultural, Food, Environmental and Animal Sciences, University of Udine, Via delle Scienze 206, Udine, 33100, Italy

Correspondence
Paolo Tarolli, Department of Land, Environment, Agriculture and Forestry, University of Padua, Agripolis, Viale dell'Università 16, 35020 Legnaro (PD), Italy.
Email: paolo.tarolli@unipd.it

Funding information
University of Padova, Grant/Award Numbers: DOR2079232, DOR1948955

Abstract

Among the environmental problems that could affect agriculture, one of the most critical is ponding. This may be defined as water storage on the surface in concavities and depressions due to soil saturation. Stagnant water can seriously affect crops and the management of agricultural landscapes. It is mainly caused by prolonged rainfall events, soil type, or wrong mechanization practices, which cause soil compaction. To better understand this problem and thus provide adequate solutions to reduce the related risk, high-resolution topographic information could be strategically important because it offers an accurate representation of the surface morphology. In the last decades, new remote sensing techniques provide interesting opportunities to understand the processes on the Earth's surface based on geomorphic signatures. Among these, Uncrewed Aerial Vehicles (UAVs), combined with the structure-from-motion (SfM) photogrammetry technique, represent a solid, low-cost, rapid, and flexible solution for geomorphological analysis.

This study aims to present a new approach to detect the potential areas exposed to water stagnation at the farm scale. The high-resolution digital elevation model (DEM) from UAV-SfM data is used to do this. The potential water depth was calculated in the DEM using the relative elevation attribute algorithm. The detection of more pronounced concavities and convexities allowed an estimation and mapping of the potential ponding conditions. The results were assessed by observations and field measurements and are promising, showing a Cohen's $k(X)$ accuracy of 0.683 for the planimetric extent of the ponding phenomena and a Pearson's r_{xy} coefficient of 0.971 for the estimation of pond water depth. The proposed workflow provides a useful indication to stakeholders for better agricultural management in lowland landscapes.

1 | INTRODUCTION

Water storage on terrain surfaces may be a serious problem in agriculture, especially in lowland landscapes. It can be described as a surplus of water that remains on the surface due to prolonged rainfall, snowmelt, or irrigation (Chen et al., 2000; Pásztor et al., 2015; Saadat et al., 2020). The negative effects are manifested in various forms. First, it causes serious damage to crops at the biological level, mainly related to the lack of oxygen supply (Gupta et al., 2004; Singh, 2015). Also, soils exposed to long ponding periods may suffer a reduction in fertility (Dunin, 2002). In this framework, the crop yield may decrease significantly (McFarlane & Williamson, 2002). Another aspect refers to the in-field accessibility at the proper time for optimal agricultural management (i.e. trafficability; Chipanshi et al., 2018).

The first cause of ponding could be found in the poor capacity of the soil to drain water, a circumstance that occurs when the water input exceeds the potential infiltration (Haghnazari et al., 2015). In particular, the soil's hydraulic conductivity is significantly influenced by texture, skeleton, aggregates, and the pore system (Archer et al., 2002; Ben-Hur et al., 2009; Saxton et al., 1986; Servadio

et al., 2001). For example, soils with high clay content are interesting, where permeability changes according to moisture conditions (Bronswijk, 1991; Yaalon & Kalmar, 1984). Also, non-optimal agricultural practices, such as heavy machinery, can worsen this condition, especially regarding soil compaction (Berli et al., 2004; Bottinelli et al., 2014; Pijl et al., 2019a). This process reduces soil porosity and permeability, leading to changes in its characteristics and behaviour (Batey, 2009; Keller et al., 2019; Soane & Van Ouwerkerk, 1994). The rising of the shallow water table due to subsurface water is also a cause of ponding (Mueller et al., 2005; Salvucci & Entekhabi, 1995). Another important factor causing water stagnation is the absence of drainage systems which can drain the water into the hydrographic network. The terrain topography may provide an important contribution, especially considering a factor such as a slope that can lead to the accumulation of runoff in specific surface concavities (Tarolli et al., 2019). Specifically, microtopography plays a key role. Indeed, terrain microstructures affect both the formation of runoff and the amount of water stored on the surface (Frei & Fleckenstein, 2014). In concave areas, the soil is rapidly subject to saturation, therefore surface stagnation can occur more frequently. This condition may easily happen in lowland fields if not properly managed.

Since topography is one of the determining factors in waterlogging, the analysis of the terrain's morphological characteristics could provide useful information for identifying potentially vulnerable areas and preventing waterlogging. Indeed, thanks to the rapid technological developments of the last decades, remote sensing offers new interesting prospects for knowledge of the Earth's surface. It becomes a strategic tool for identifying critical issues during agricultural production and provides support for designing sustainable solutions. High-resolution topography (HRT) techniques permit different opportunities to investigate agricultural surfaces, allowing 3D reconstruction of even the smallest surface signatures. HRT may be performed using diverse acquisition platforms (Cucchiaro et al., 2020; Gupta, 2017; Xue et al., 2008). For example, LiDAR allows the topographic reconstruction of an agricultural landscape at large spatial scale through an airborne laser scanner (ALS; Ladefoged et al., 2011; McCoy et al., 2011) or at a detailed scale, through a terrestrial laser scanner (TLS; Barneveld et al., 2013; Eitel et al., 2010). Nowadays, a rapid and low-cost solution is the structure-from-motion (SfM) photogrammetry technique paired with multi-stereo view (MSV) algorithms (hereafter SfM). This has been used in different studies in agriculture: to analyse microtopography on surfaces managed with conservation agricultural management (Tarolli et al., 2019); to monitor the bank erosion in drainage network (Prosdocimi et al., 2015); to measure the surface roughness of cultivated terrain surfaces (Martinez-Agirre et al., 2020; Snapir et al., 2014); and to estimate soil loss by erosion (Vinci et al., 2017). SfM may be used through different acquisition platforms that permit analysis at different spatial levels, from plot to field scale (Dong et al., 2017; Jay et al., 2015; Nguyen et al., 2016). For larger-scale surveys, the use of UAVs (unmanned aerial vehicles or drones) allows the realization of high-resolution DEMs, indispensable support for the knowledge of the processes taking place on agricultural surfaces. For example, they are used in agriculture to map erosion and deposition (Meinen & Robinson, 2020); identify potentially unstable areas due to surface runoff and provide suitable solutions (Pijl et al., 2019b); measure the height of crops (Chang et al., 2017); and estimate the biomass (Bendig et al., 2014; Gil-Docampo et al., 2020). A DEM rich in detail and capable of describing terrain signatures opens up considerable opportunities for understanding the processes occurring on it. It may also be a useful tool in understanding the surface water storage phenomena. Tarolli et al. (2019) proposed an innovative and effective method to evaluate stagnant water's potential depth on an agrarian surface using small experimental plots (2×2 m) and a DEM of 0.02 m pixel resolution derived using a handled mirrorless camera. However, they did not test the method at a larger scale or validate it with real ponding conditions. Other literature examples where DEMs have been used for similar purposes concern the investigation of snow patterns in agricultural landscapes (Lapena & Martz, 1996), laboratory analysis for water storage quantification (Chaplot & Le Bissonnais, 2003; Kamphorst & Duval, 2001; Ullah & Dickinson, 1979), or catchment-scale waterlogging analysis in agriculture (Merot et al., 1995).

This work aims to provide a robust, rapid, and low-cost method for mapping ponding on an entire farm's soil surface. To do this, a methodology based on a high-resolution DEM (0.10 m cell) derived from UAV-SfM is proposed. To our knowledge, UAV use for detecting ponding in agriculture is a novelty. Specifically, this approach investigates the terrain's signatures through a geomorphological indicator able to map the depressed areas of the terrain. For those areas, morphologically prone to water ponding, the spatial extent and the potential waterlogging depth were detected. The quality of the mapping was then compared with a solid statistical assessment based on a detailed field survey campaign, considering real ponding conditions.

2 | STUDY AREA

The study area is located within the municipality of Rovigo (RO), in northern Italy (45°06′07″N; 11°52′10″E; Figure 1a). It is a lowland area (slope < 1%), devoted to agriculture and historically subject to land reclamation, as well as numerous territories of the Po and Adige Valley (Curtis & Campopiano, 2014). Over the last years, the average annual precipitation was 750.4 mm, with a peak in 2013 of 1006.4 mm. The rainiest month was May, with an average cumulated rainfall of 84.8 mm (ARPAV, 2020). The phenomenon of standing water in the field was reported all across the year in the more depressed area. Typically, it remains on the terrain surface from a few days to a week, and more frequently during spring and autumn. These periods were also the rainiest, with more than 200 mm per season. This fact was particularly critical for management, as sowing is usually scheduled in April. Indeed, the presence of pond water on the surface may cause delays in working time, widespread absence of seed germination, and seedling mortality.

The study area is cultivated with maize, soya, and wheat, embracing the conservation agriculture (CA) farming system (Hobbs et al., 2008; Carretta et al., 2021). No-tillage operations were carried out in the field, and the crops are harvested using agricultural machinery. The area is divided by a network of ditches (Figure 1b), and at the time of the survey, it was free of crop coverage. According to the regional soil map (ARPAV, 2019), the zone is characterized by soils originating from the depressed region of the alluvial plain and mainly composed of silt and clay. Moreover, it is characterized by a high available water capacity (AWC, 225–300 mm) and moderately low permeability (0.36–3.6 mm/h). The condition of topographic depression, in

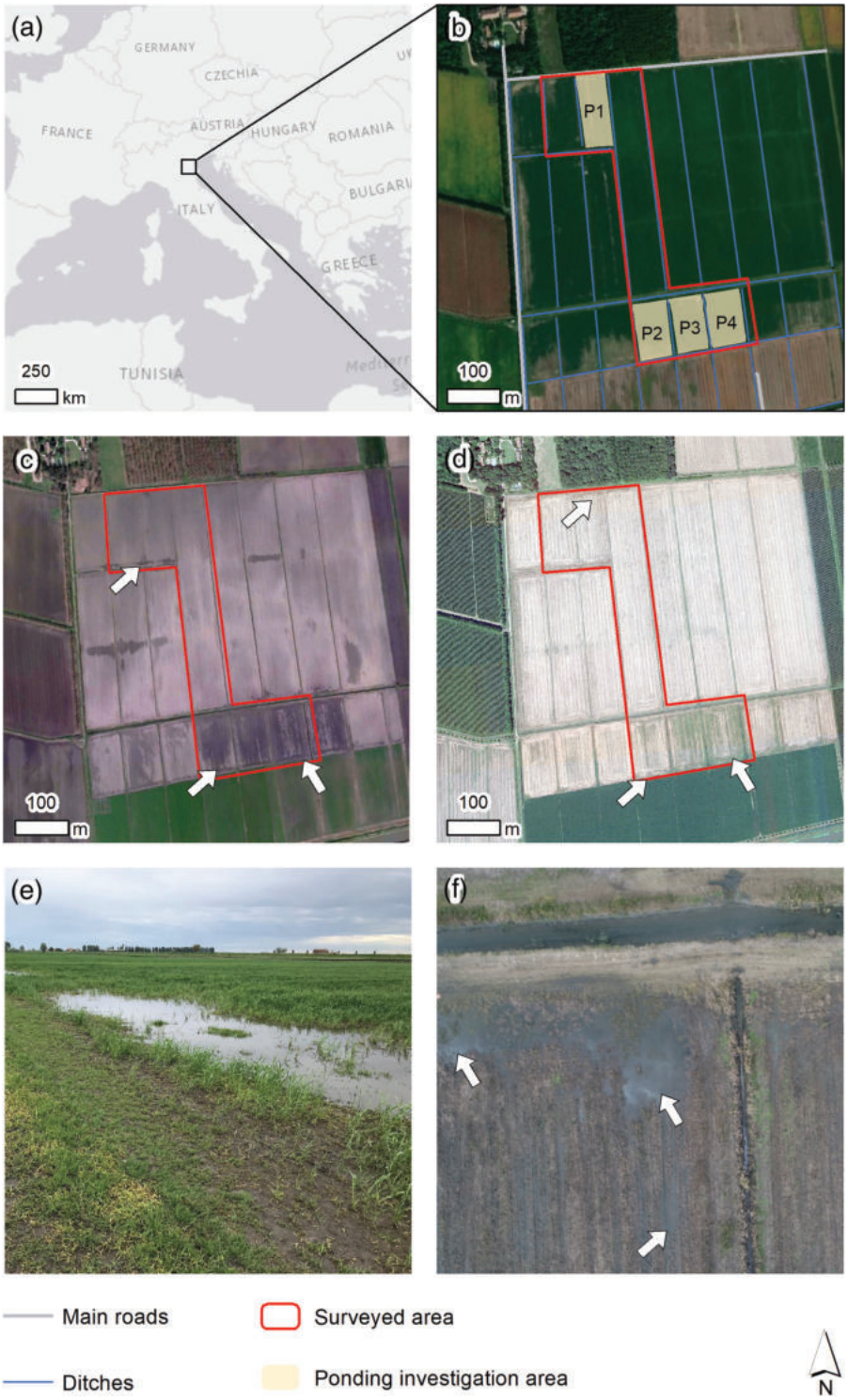

FIGURE 1 (a) Territorial framework of the study area (Rovigo, northern Italy). (b) The area surveyed by UAV-SfM and plots for water ponding analysis (P1, P2, P3, P4). The ditches/roads network is drawn on an orthophoto provided by Esri® (2016). (c, d) Orthophotos provided by Google® from 2015 and 2018, respectively. Arrows indicate problems affecting crops related to water ponding. (e) Water ponding from the field. Photo by Sofia Michieli. (f) UAV picture that shows wet zones in the study area. Arrows indicate some ponded areas. Photo by Sara Cucchiaro [Color figure can be viewed at wileyonlinelibrary.com]

addition to soil properties, makes the area easily susceptible to surface water stagnation. This fact is also observable from the past years' orthophotos (2015 and 2018) reported in Figures 1c and d, where areas of different colour are visible. Ponding is also evident in Figures 1e and f. This work investigates the areas where the phenomenon has been observed in the past (P1, P2, P3, P4 in Figure 1b).

3 | METHODS

The presented method for potential surface ponding mapping involved a first phase of in-field campaign for data collection. Subsequently, various tools were used for data processing, mapping, and result assessments. The workflow that describes the main conceptual steps is proposed in Figure 2.

3.1 | Data acquisition and analysis

The photogrammetric survey (Figure 2, A1) was performed after the harvest period, to ensure optimal conditions for applying the SfM technique, showing the agricultural surface as free as possible from vegetation. The survey was carried out using a DJI Zenmuse X4S camera (20M pixels, focal length 8.8 mm, 1-inch CMOS sensor) mounted on a professional quadcopter (DJI Matrice210v2). The drone was parametrized to provide 70% side–85% front picture overlap,

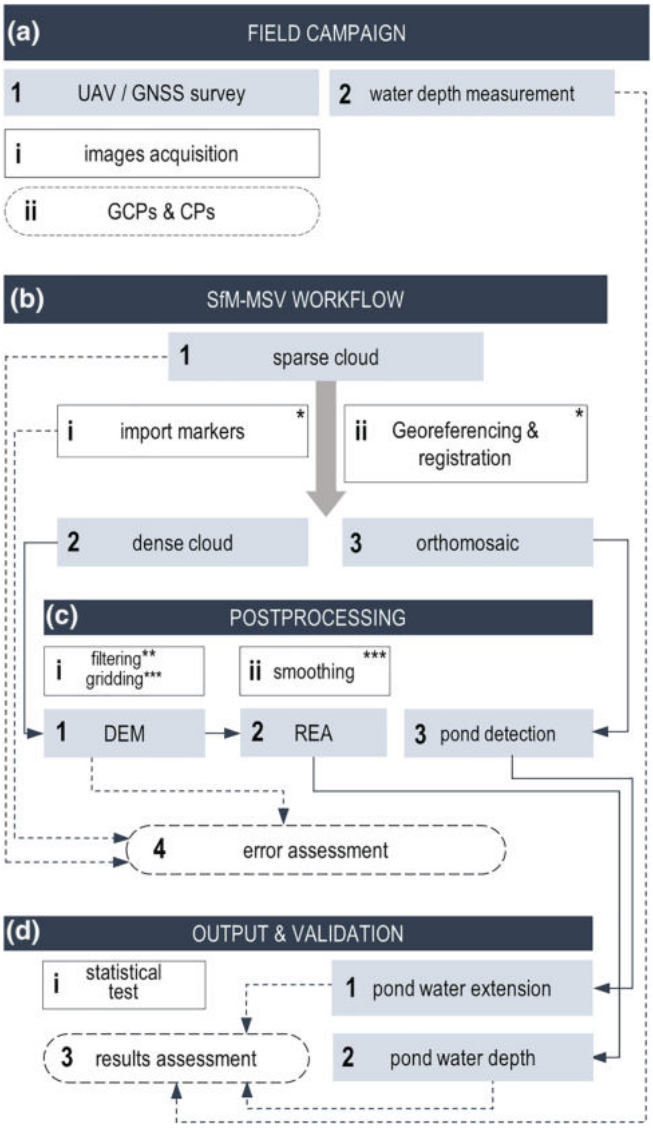

FIGURE 2 Workflow for potential water ponding mapping in agriculture using UAV-SfM. In detail, the diagram shows the process from in-field data acquisition to SfM-MSV steps, post-processing and output generation/validation. * Refers to the use of Agisoft PhotoScan Pro® 1.4.5 software; ** refers to CloudCompare software; *** refers to Esri ArcGIS® Desktop (version 10.6.1.9270) software [Color figure can be viewed at wileyonlinelibrary.com]

essential for the image-matching algorithms used in SfM (Eisenbeiss & Sauerbier, 2011; Eltner et al., 2016). Considering the flat morphology of the study area, free of complex features requiring specific analysis, the flight was performed in automatic mode. The UAV followed a route consisting of 16 strips and took nadiral photos (Figure 2, Ai). The survey covered a wider area than the water ponding investigation zones only, including the region between northern and southern plots. Before the acquisition of the images, ground control points (GCPs) and check points (CPs) were placed in the study area (Figure 2, Aii; Figure 3). They were disposed of directly in the field, attempting to maintain a homogeneous distribution, avoiding the formation of clusters or preferential lines. GCPs were used in the georeferencing and registration processes (Figure 2, Bi, Bii) to improve the 3D reconstruction of the terrain surface, while CPs were used for results validation. The *xyz* coordinates of ground points were measured with a Geomax Zenith40 GNSS (Global Navigation Satellite System) in Real-Time-Kinematic (RTK) mode (WGS84/UTM zone 32 N, EPSG: 32 632 coordinate system). This step was essential to georeference the SfM outputs and evaluate the photogrammetric errors (Grayson et al., 2018). Table 1 describes the main information about the UAV-SfM survey.

3.2 | Data processing

Before image processing, pre-calibration of the drone camera was carried out using Agisoft Lens® software. This preliminary step allowed an automatic lens calibration routine using an LCD screen as a target. In this way, it was possible to estimate the camera model parameters and lens distortion coefficients. Then, this information was refined in the SfM step, where the pictures dataset was processed using the photogrammetric software Agisoft PhotoScan Pro® 1.4.5. This extracts 3D point clouds from the images and orthomosaics based on SfM and MVS algorithms (James et al., 2017; Javernick et al., 2014). In the first step, the software was able to generate and display a sparse point cloud (Figure 2, B1). This phase was important for the photogrammetric workflow, as by observing it and the errors of the tie points it was possible to recognize systematic problems that would otherwise be propagated in the next steps. For this reason, Phonoscan's command 'Gradual selection' was used to identify and delete points characterized by high error. Subsequently, the bundle adjustment was performed. This operation refines the positions of the cameras and tie-points using the calibration parameters. This algorithm improves the values during the image alignment phase by removing outliers and mismachining from the sparse point cloud. The georeferencing of the 3D point cloud was carried out using the traditional solution of the GCP coordinates (Carrivick et al., 2016). The SfM process uncertainty assessment was evaluated on the sparse cloud using GCPs and CPs (Figure 2, C4), considering the residuals of each point (i.e. the difference between the real coordinates of this point measured with the GNSS in the field and the modelled SfM values). The mean of the residuals indicates the accuracy of the registration process and the point cloud when the GCP and CP residuals are considered. Also, the standard deviation of the residuals' yields indicates the precision (Cucchiaro et al., 2018). To finish, other metrics such as the root mean square error (RMSE) were calculated for the three directions *x*, *y*, *z* (i.e. $RMSE_{3D}$) for the vertical error ($RMSE_Z$) and the planar ones ($RMSE_{XY}$) as described in Remondino et al. (2017). These statistics provided an opportunity to check all potential bias in the point cloud.

Starting from the sparse cloud, the dense point cloud was processed using the MSV algorithm in Agisoft PhotoScan Pro® 1.4.5 (Figure 2, B2), as well as the orthomosaic (0.05 m resolution; Figure 2, B3). The dense cloud was then imported into CloudCompare software (Omnia Version 2.10.2; http://www.danielgm.net), to be post-processed and filtered through different steps (Figure 2, Ci). First, the outliers have been removed, eliminating noise but preserving the surface features (Han et al., 2017). This operation was performed through the Statistical Outliers Removal (SOR) filter. Afterwards, the point cloud was filtered manually, removing all points not belonging to the terrain (Jensen & Mathews, 2016). Where the UAV-SfM technique failed in detecting the ground in critical spots (in particular dense crop residues), some points belonging to low ground cover were left to avoid unrealistic information gaps in the final output.

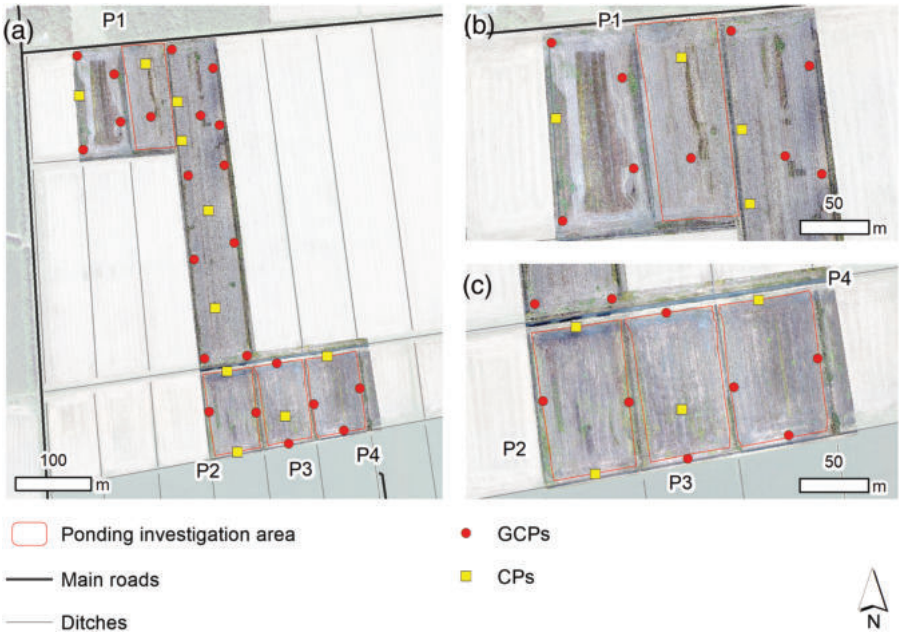

FIGURE 3 Spatial distribution of GCPs/CPs and the four plot locations for the ponding analysis on the 0.05 m resolution orthomosaic. In the background, an orthophoto provided by Google®. (a) The entire area surveyed by UAV-SfM; (b) focus on P1; (c) focus on P2, P3, P4 [Color figure can be viewed at wileyonlinelibrary.com]

TABLE 1 Main characteristics of UAV-SfM acquisitions

Covered area (ha)	Number of images	Flight height (m)	GSD[a] (m)	Number of tie points	Number of GCPs (CPs)	GNSS positional accuracy (*x*, *y*, *z*) (m)
7.92	542	50	0.0148	3,107,333	22 (10)	0.02–0.03

[a]Ground sample distance (GSD) value calculated according to Neumann (2008).

These problematic areas were limited, however, and did not alter the final water ponding mapping. The points of the filtered dense cloud were finally interpolated and gridded within Esri ArcGIS® Desktop (version 10.6.1.9270) software using the Natural Neighborhood Interpolation algorithm to create the DEM (Garnero & Godone, 2013; Sibson, 1981; Figure 2, Ci, C1). This method was selected because it can leave a rougher terrain morphology, avoiding the smoothing effects given by other techniques (Pirotti & Tarolli, 2010). Indeed, a rougher and more realistic surface could detect even the smallest concavities, thus helping in ponding detection.

Error assessment was performed for both sparse point cloud and DEM, generated after dense cloud filtering (Figure 2, C4). Indeed, the transformation of a cloud into a gridding elevation surface introduced several uncertainties or artefacts that influence the accuracy/quality of the produced surface. Therefore, in particular in the vertical component, these errors were evaluated through a statistical comparison between the Z values of CPs (measured in the field by GNSS) and the equivalent Z measures of DEMs. First, following Höhle and Höhle's (2009) approach, the outliers were removed by applying a threshold selected from an initial calculation of the error measures. Then, RMSE (Estornell et al., 2011), standard deviation (SDE), mean error (ME), and the normalized median absolute deviation (NMAD), a robust estimator for the SDE more resilient to outliers in the dataset (Cucchiaro et al., 2020; Gonçalves et al., 2018; Höhle & Höhle, 2009) were calculated.

3.3 | Relative elevation attribute

The REA (Figure 2, C2) is a morphometric indicator calculated as (Carturan et al., 2009):

$$REA_r = \overline{E_r} - E_{DTM_r} \quad (1)$$

$\bar{E}_r$ is the average elevation within a kernel around the grid cell with elevation E_{DTM_r}. The central idea is to apply a low-pass filter to the DEM, thus obtaining a smoothed version of the original surface (Figure 2, Cii). By subtracting the DEM from the latter, a map highlighting the local reliefs and depressions is obtained. Since the REA has been successfully applied by Tarolli et al. (2019) to map the potential surface water stagnation phenomena in small experimental plots, this study proposes an upscale to farm level. In detail, the REA was calculated based on the high-resolution DEM (0.10 m cell) from the UAV-SfM survey. Its smoothed version was obtained using a kernel around the grid cell, chosen according to the size of the morphological signatures investigated, such as areas in subsidence due to the transit of agricultural vehicles and prone to water ponding. Specifically, a moving window of 71×71 cells was selected, with a size of about two to three times the extent of the features, as proposed by Tarolli et al. (2012). The REA was able to map the planimetric extent of these critical areas and offer a vertical depth value expressed as residual relief. Assuming that stagnant water is mainly formed in the surface's concavities, the use of the REA aims to exploit the altitude variation between the two DEMs to provide a water depth measure. The method is optimal if the survey is carried out with bare soil without ponding on the surface. In this way, the terrain morphology is the determining factor for stagnant water's appearance, permitting the mapping of the maximum ponding condition. Historical orthophotos built for particularly intense ponding events could also be useful for validation purposes. However, the REA could potentially be used at different periods of the year if there are suitable surface cover conditions for UAV-SfM. Indeed, it offers a quick, low-cost, and

effective overview of the waterlogging phenomena at farm scale and the possibility of timely result assessments with orthomosaics. In other geoscience contexts, the REA was also used effectively to understand the wind exposure in glacier analysis (Carturan et al., 2009; Cazorzi et al., 2013), detect the agricultural hydrographic network, and estimate the water storage capacity of anthropogenic landscapes (Sofia et al., 2014).

3.4 | Statistical validations

The ponding value estimated by the REA indicator was statistically assessed to test if there is a positive correlation with what is observed in the field (Figure 2, D3, Di). Two different analyses were performed. The first one aimed to verify if a pixel classified as ponding by the REA falls in water stagnant areas observable in the 0.05 m orthomosaic (Figure 2, D1). The second one researched a correlation between the water depth estimated by the indicator (Figure 2, D2) and the water depth measured in the field by a stick meter in 47 sample points (Figure 2, A2).

3.4.1 | Spatial distribution accuracy assessment

Regarding the first analysis, in which the area covered by pond water is investigated, the REA raster was classified into two classes assigned binary values: 'Ponding' (water depth > 0 m) and 'No ponding' (water depth ≤ 0 m), from now on called the 'comparison raster'. To assess its accuracy, the REA raster was compared to the 'reference raster' obtained by digitizing shapefile polygons drawn manually based on the orthomosaic in areas where pond water was present (Figure 2, C3). This raster was then reclassified using binary values, as for the comparison raster. Consequently, the statistical comparison was done by Cohen's kappa standard accuracy, able to control chance agreement by incorporating all marginal distributions of an error matrix (Cohen, 1960). Table 2 shows the format of the confusion matrix (X) used for the assessment (Stehman, 1996; Pirotti & Tarolli, 2010; Pontius & Millones, 2011; Stehman, 1996).

The i and j elements are the number of rows (based on the comparison raster) and columns (based on the reference raster) that correspond to the number of classes used for the analysis. In contrast, elements n are the result of pixel comparison between input data. The matrix was subsequently normalized as described in Equation 2, so that each of its elements n will be expressed as a function of the total number of pixels p (Pontius & Millones, 2011):

$$p_{ij} = \left(\frac{n_{ij}}{\sum_{j=1}^{J} n_{ij}}\right)\left(\frac{N_i}{\sum_{i=1}^{J} N_i}\right) \quad (2)$$

where p represents the normalized value of the n_{ij} element in the original matrix, J is the number of classes, and N_i is the total number of pixels for each row. Based on the normalized version of the confusion matrix X, Cohen's kappa standard accuracy $k(X)$ is calculated as:

$$k(X) = \frac{C - E}{1 - E} \quad (3)$$

Here, C is the proportion agreement, calculated as the normalized sum of true positive pixels, and indicator of concordance:

$$C = \sum_{j=1}^{J} p_{jj} \quad (4)$$

According to Pontius and Millones (2011), E is instead the overall expected agreement. It is calculated assuming a random spatial allocation of the classes in the comparison raster, given the proportions of those classes in the reference and comparison raster. The expected agreement (e_g) for an arbitrary class g is proposed in Equation 5, while E in Equation 6 refers to their sum:

$$e_g = \left(\sum_{i=1}^{J} p_{ig}\right)\left(\sum_{j=1}^{J} p_{gj}\right) \quad (5)$$

$$E = \sum_{g=1}^{J} e_g \quad (6)$$

3.4.2 | REA and in-field measurement: water depth assessment

During the survey, the depth of the stagnant water on the agricultural surface was measured at 47 sample points using a stick meter and their positions are shown in Figure 4.

TABLE 2 Confusion matrix (X) presented by Pontius and Millones (2011) and used to evaluate the accuracy with which the proposed method can map water ponding

		Reference[b]					
		j = 1	**j = 2**	**...**	**j = J**	**Sample total**	**Population total**
Comparison[a]	$i = 1$	n_{11}	n_{12}		n_{1J}	$\sum_{j=1}^{J} n_{1j}$	N_1
	$i = 2$	n_{21}	n_{22}		n_{2J}	$\sum_{j=1}^{J} n_{2j}$	N_2
	...						
	$i = J$	n_{J1}	n_{J2}		n_{JJ}	$\sum_{j=1}^{J} n_{Jj}$	N_J

[a]Comparison refers to the binary raster based on the REA.
[b]Reference refers to the rasterization of the polygons identifying the presence of pond water in the field derived by the orthomosaic.

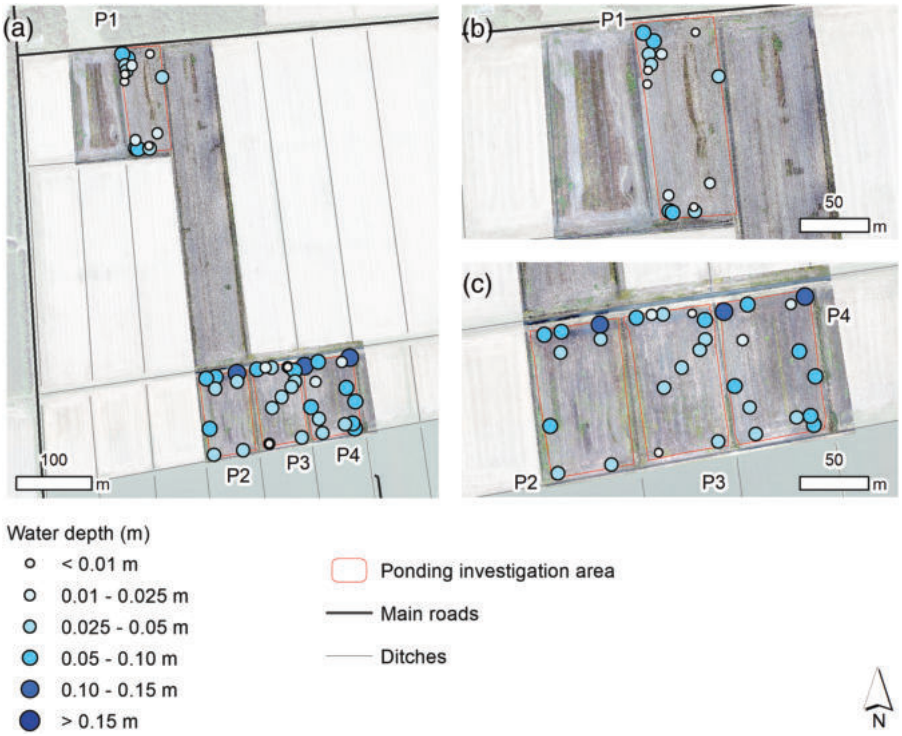

FIGURE 4 Spatial distribution of the in-field measurements of the pond water depth (measured by a stick meter) on the 0.05 m resolution orthomosaic. For better data visualization on the map, points are themed with a colour scale (from light blue to blue) and with variable size (from small to large) for increasing depth observations: (a) the entire area surveyed by UAV-SfM; (b) focus on P1; (c) focus on P2, P3, P4 [Color figure can be viewed at wileyonlinelibrary.com]

These effective depth measurements were statistically compared with what was estimated using the morphological approach investigated. Indeed, the degree of correlation between the two quantitative variables was evaluated, which was necessary to validate the methodology's reproducibility (Lin, 1989). The Pearson coefficient r_{xy}, also known in statistics as bivariate correlation, was used. This indicates a linear correlation between two variables, its direction, and how statistically robust the agreement is (Adler & Parmryd, 2010). Equation 7 was used to verify the correlation between real and estimated water depth measurements. In general, positive values describe a linear relationship, with a maximum value of 1 that defines a perfect match:

$$r_{xy} = \frac{cov\,(x,y)}{\sqrt{var(x)} \cdot \sqrt{var(y)}} \tag{7}$$

where $cov(x,y)$ is the sample covariance between two variables x (water depth measured in the field) and y (water depth estimated by REA); $var(x)$ and $var(y)$ are the respective sample variances. In addition to the coefficient's measurement, the relationship between the two variables is proposed in the form of scatterplots (one for each study plot P1, P2, P3, P4), to graphically appreciate correlation.

4 | RESULTS AND DISCUSSION

4.1 | UAV-SfM processing

The processing of SfM data allowed the generation of a detailed point cloud (mean density of 1728 points/m^2), an orthomosaic of the study area with 0.05 m resolution (used to interpret the presence of pond water in the field), and a high-resolution DEM at 0.10 m. Furthermore, Figure 5 shows an overview of the site presenting some vegetation and crop residual points, as well as two examples of cross-sections (Figures 5a–c).

Figure 6 shows the shaded relief map obtained from the SfM DEM, thematized according to the elevation and the four investigation areas (P1, P2, P3, P4) where ponding analysis was performed.

Tables 3 and 4 show the error analysis of the UAV-SfM point cloud and the DEM of the study area, respectively.

As can be observed from the evaluation of the errors, the SfM technique has proved to be valid and robust in the digital reconstruction of the elevation. Furthermore, during the interpolation and gridding process of the point cloud, different interpolation techniques could be tested to further mitigate errors, but this analysis is too specific for this paper's scope. Indeed, the choice of the appropriate interpolation algorithm is a debated issue in the literature, as well as the optimal neighbourhood size setting (Milenković et al., 2015). However, the DEM generated following the proposed procedure was suitable for the aim of this research, offering high-resolution and quality data.

4.2 | REA application

Figure 7 reports the calculation of the REA indicator. It allows the identification of depressed areas, highlighting concavities and convexity of the surface and for this reason, it can be used to estimate the potential presence of stagnant water.

As can be observed in Figure 7, the maps indicate higher values of stagnant water depth mainly along the borders of the study areas (a phenomenon particularly evident in P1 and P4). This is related to the terrain's concave profile, which causes the concentration of water in specific areas, where it is mainly drained thanks to the soil's infiltration capacity. This fact is the central cause of ponding for this site and is also linked to the management chosen for the field. In a regime of

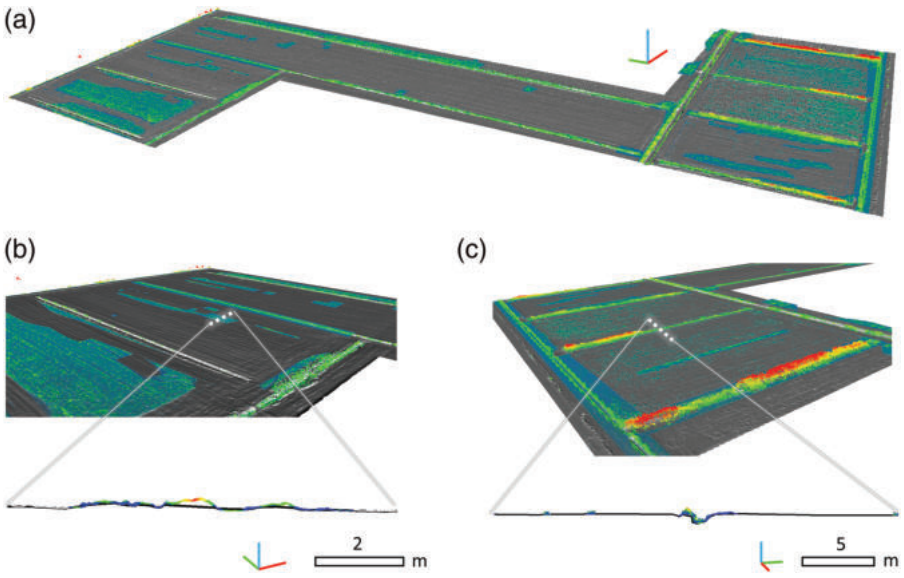

FIGURE 5 (a) Point cloud of the entire study area. In a blue-to-red colour scale, points belonging to the vegetation and crop residual are displayed according to their distance to the ground level; (b) an enlargement of the upper part of the site, showing a cross-section passing through a spot covered by crop residues; (c) another enlargement with a cross-section passing over a ditch [Color figure can be viewed at wileyonlinelibrary.com]

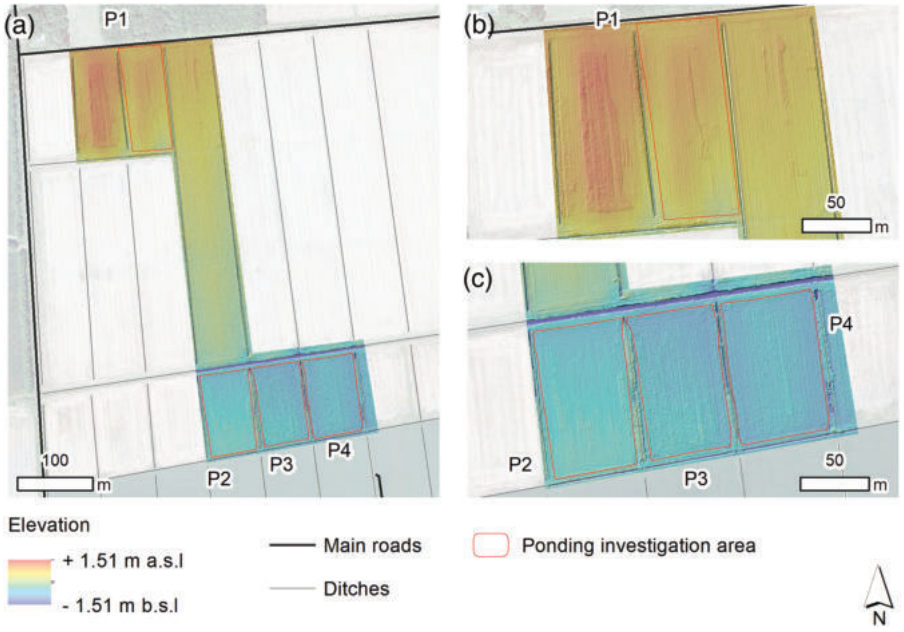

FIGURE 6 (a) Shaded relief map of 0.10 m DEM, thematized according to the elevation for the entire study area surveyed by UAV-SfM; (b) focus on P1; (c) focus on P2, P3, P4. As can be seen, part of the study area is located below sea level. Indeed, it is included in the reclaimed land of the Rovigo province [Color figure can be viewed at wileyonlinelibrary.com]

TABLE 3 Error assessment of the UAV-SfM point cloud, as described in the text. Calculated on the values exported from Agisoft PhotoScan Pro® 1.4.5 for the sparse cloud, after cloud refinement and bundle adjustment. Data elaborated by comparing the photogrammetric processing results with the in-field GNSS position measures of CPs and GCPs. Values calculated on CPs are considered as accuracy (MAE and $RMSE_{3D}$) and precision (SDE), while on GCPs as registration errors ($RMSE_{3D}$)

Accuracy CPs				Precision CPs			Registration GCPs
MAE (m)			$RMSE_{3D}$ (m)	SDE (m)			$RMSE_{3D}$ (m)
X	Y	Z		X	Y	Z	
0.010	0.011	0.030	0.021	0.005	0.004	0.029	0.034

TABLE 4 Error statistics of the UAV-SfM DEM. Data elaborated by comparing the cell values of the DEM with the Z values of CPs

MAE (m)	ME (m)	SDE (m)	RMSE (m)	Median (m)	NMAD (m)
0.014	0.001	0.017	0.038	−0.003	0.023

minimum soil disturbance, it was decided not to till the terrain. But in this way, the soil has undergone compaction, with consequent porosity reduction and subsidence, a fact already reported in other studies (Nunes et al., 2015; Suzuki et al., 2013).

In contrast, in the plots' central areas, it is easy to observe water stagnation caused by soil compaction (mainly in P2 and P3). Due to the pressure exerted by the mass of vehicles during harvesting, this phenomenon causes local subsidence and reduces the water

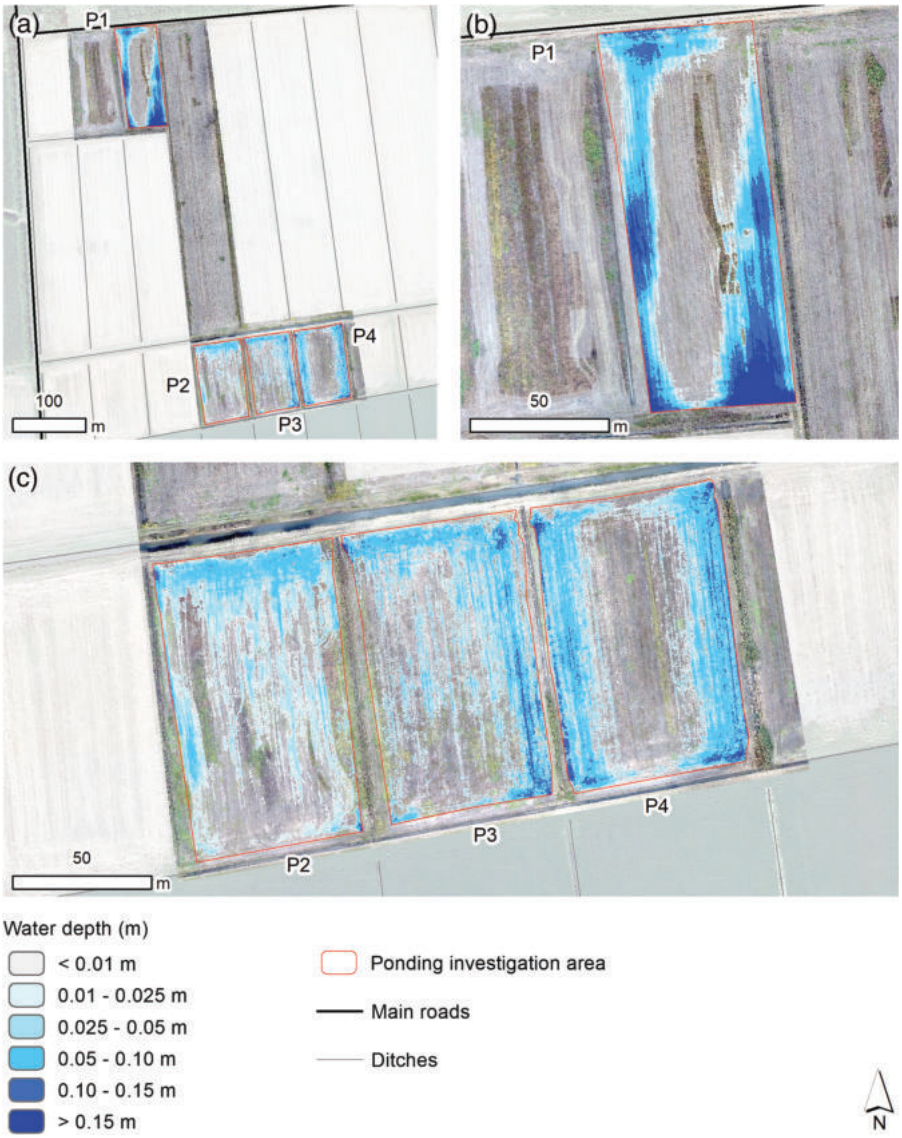

FIGURE 7 Potential pond water depth estimated on a 0.10 m DEM through the REA indicator. The raster is classified into water-depth classes to which a colour is assigned (transparent for 'No ponding'). (a) Whole study area; (b) focus on plot P1; (c) focus on plots P2, P3, P4. Particularly interesting are the blue stripes that are evident in the middle of these plots, created due to heavy mechanization [Color figure can be viewed at wileyonlinelibrary.com]

infiltration capacity of the soil (Horn et al., 1995). Stagnations of a few metres wide can be observed (in some cases less than 1 m), which extend along the direction of the maximum plot length. Finally, although this is not the main purpose of this work, it is also important to mention the role of soil type and its propensity to be waterlogged. As described earlier, the soil in the study area mainly consists of clay and silt, with moderate permeability and formed in depressed alluvial zones.

In this context, appropriate solutions may concern the use of drainage systems. Several studies in the literature illustrate how they may be used to combat waterlogging in agriculture. For example, Singh (2017) provides an overview of different drainage technologies; Ritzema et al. (2008) test several subsurface drains to counteract stagnation in irrigated land in India, according to soil type and annual rainfall; other applications are described for case studies in Australia (Cox & McFarlane, 1995), Pakistan (Qureshi et al., 2008), and Turkey (Bahçeci & Nacar, 2009). Also, another solution consists of modifying the profile of the agricultural surface through appropriate soil movements. In this way, by working on the topography, it is possible to avoid depressed areas and create a slope gradient that drains the water runoff towards the ditches. In this regard, other research has investigated the potential of a correct combination between field topography and ditches (Appels, 2013; Dunn & Mackay, 1996; Shore et al., 2013), leading to efficient water management and the solution of waterlogging.

TABLE 5 Summary table of the statistical assessment described in the text. According to Pontius and Millones (2011): C (dimensionless), used in the calculation of k(x), is the proportion agreement; E (dimensionless), used in the calculation of k(x), is the overall expected agreement. According to Cohen (1960): k(x) (dimensionless) is the kappa standard and measures the accuracy with which the proposed approach can predict the extension of the area potentially occupied by pond water. r_{xy}, Pearson's coefficient (dimensionless), measures the correlation between the water depth measurements made in the field at sample points and the values predicted by the proposed approach

Plot	C [–]	E [–]	k(x) [–]	r_{xy} [–]
P1	0.856	0.500	0.712	0.991
P2	0.810	0.497	0.622	0.994
P3	0.806	0.495	0.616	0.963
P4	0.891	0.501	0.782	0.938
Average	0.841	0.498	0.683	0.971

4.3 | REA assessment

Regarding the assessment of the results, the two statistical tests described above are performed. Looking at the first analysis, it is possible to observe in Table 5 and Figure 8 how the proposed method can map the extent of the area potentially subject to water ponding with a reasonable estimation. It is interesting to note the high value of $k(x)$, an indicator of concordance, which shows how the REA can classify a pixel as ponding in an acceptable way. The second statistical assessment shows an important correlation between the two datasets (Table 5), also confirmed by scatterplots in Figure 9. Looking at these, a positive correlation can be observed between the values measured in the field and those estimated by the method, with a variance tending to remain within the confidence interval displayed. This is mainly the case for P1 and P2, where higher values of r_{xy} were found than for P3. In P4, a more noticeable discrepancy may be observed. Looking at Figure 9d, it is possible to note an underestimation of the stagnant water depth for lower values and an overestimation for higher values. Specifically, there is one point where the estimated depth of standing water is about 6 cm greater than that measured.

The proposed method is affected by limitations that may influence the water depth estimation, especially if some standing not-clear water remains on the surface. Being a purely geomorphological approach, soil and surface water characteristics and weather conditions are not considered input. For this reason, it is assumed that the same starting conditions exist throughout the study area. Indeed, this work aims to offer stakeholders a quick and cost-effective standing water mapping tool; implicit approximations are therefore inevitable but acceptable, considering that a complex problem is described with an expeditious methodology. Also, limitations can be found in the instruments and methodologies used to perform the survey and to process the data. The first limit regards the point cloud's errors,

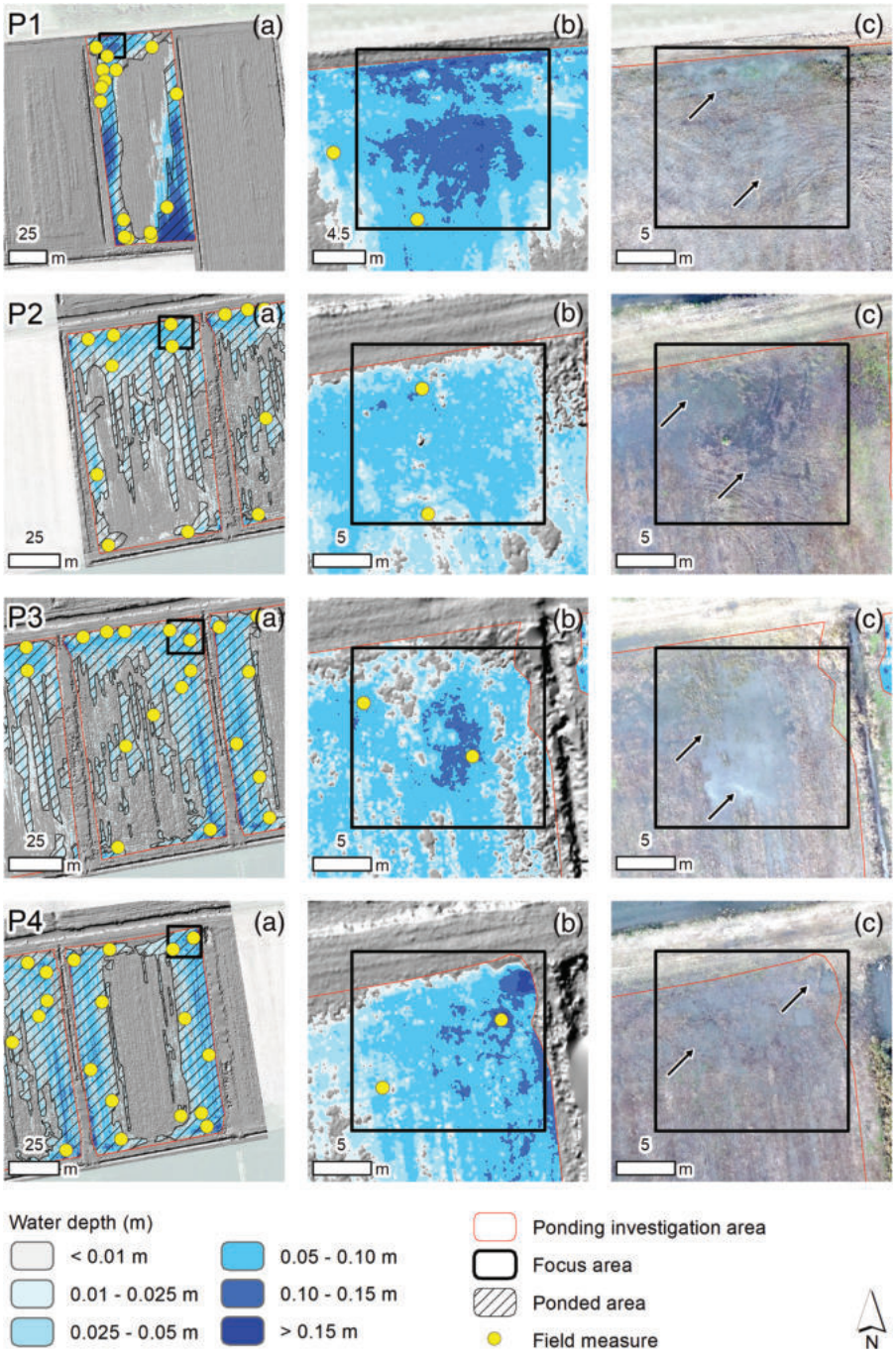

FIGURE 8 Maps showing the elements used for the statistical assessment of the results. Each row corresponds to the analysis of one of the four study plots. The maps in column (a) show the entire plot and indicate the position of a box ('Focus area') enlarged in columns (b) and (c). Dots are the positions where the pond water depth was measured (see Figure 4), used as a reference for the bivariate statistics. Black arrows indicate some interesting areas subject to agricultural ponding [Color figure can be viewed at wileyonlinelibrary.com]

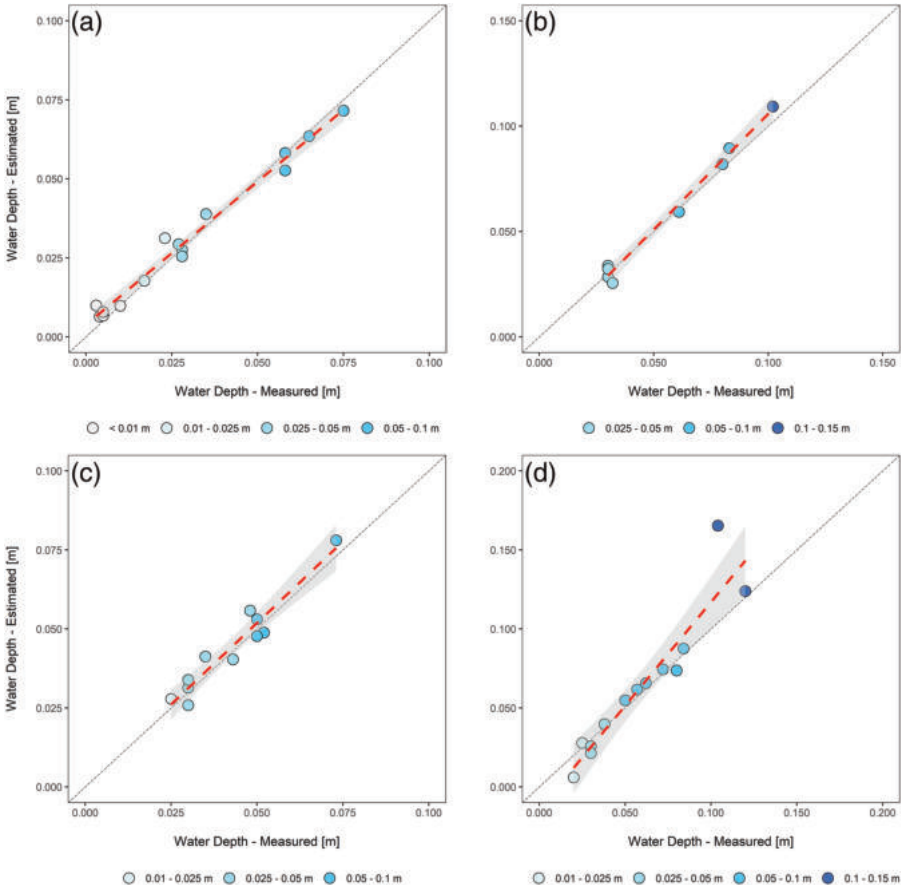

FIGURE 9 Scatterplots generated comparing the water depth measured in the field with that estimated by the REA: (a) P1; (b) P2; (c) P3; (d) P4. Graphs include the linear correlation line (95% confidence interval). Points are themed using the chromatic scale in Figures 4, 6 and 7 and based on the measured value. Elaboration was performed using R-4.0.1 for Windows (R Core Team, 2000) through the ggplot library (Wickham, 2016) [Color figure can be viewed at wileyonlinelibrary.com]

derived from the SfM processing, especially concerning the vertical coordinate (z). It is possible to improve this condition by modifying the parameters with which the survey is carried out. Specifically, the flight altitude could be lowered and the number of GCPs increased, obtaining a larger number of photographs with a better GSD. However, this causes a strong increase in the required calculation capacity for photogrammetric processing, increasing the time and cost needed to obtain the results. Another limit could be found in the point cloud cleaning phase. Especially in areas where residual vegetation was present during the survey, filtering is a very delicate and error-prone operation. In such areas, altered water depth values are more likely to be discovered. To avoid this problem, the survey should be carried out after complete cleaning of the field from vegetation and crops, an operation that is not always possible. An alternative, interesting approach could be to use aerial LiDAR for DEM generation, which can better penetrate the vegetation, providing a more complete overview of the terrain in difficult areas. However, in this case, the costs increase to outstrip the work's aim.

Finally, it is important to consider the error in the final DEM, which is propagated from the point cloud and amplified by the filtering, interpolation, and gridding operations. This issue could be more problematic if there are vegetation patches in the field. To mitigate this problem, more detailed analysis may be performed to test different interpolation techniques, also changing the neighbourhood size parameter and repeating error assessments. All these factors affecting the DEM also impact the subsequent calculation of the geomorphological indicators such as the REA, becoming a limitation in stagnant water mapping in lowland agriculture.

Other research in the literature deals with mapping areas prone to water ponding using remote sensing techniques. For example, Merot et al. (1995) tested a topographic approach. The authors mapped waterlogging in agriculture using the saturation overland flow concept proposed by Beven and Kirkby (1979), and implemented in the TOPSOIL model. Different from this paper's method, it increases the complexity of the methodology and data processing time considerably. Then, they used a 40 m resolution DEM derived from topographic 1:25 000 maps, suitable for a catchment scale, but a limit for field-scale analysis. Also, Mandal and Sharma (2001) and Pandey et al. (2012) proposed a different remote sensing approach, namely the use of multispectral satellite imagery, tested for a large-scale lowland irrigated landscape. Their analysis permitted the mapping of potentially susceptible areas to water ponding at regional and subregional scales. A similar methodology was also proposed by Liu et al. (2018), which analysed areas prone to waterlogging using commercial satellites' multispectral products. Although this methodology is widely used in the literature, some limitations may be found for water ponding mapping. Indeed, they mainly described the spatial extent of the standing water at large scale. Instead, by adopting a geomorphological method such as the one proposed in this study, it is also possible to map the depth of surface water at farm scale, thus offering the stakeholders important information for better management. Furthermore, the spatial resolution of these data is another interesting issue. Although multispectral imageries with pixels smaller than 1 m are available on the market, the detail is still insufficient to map ponding phenomena at microtopographic level. To overcome this problem, it would be useful to use a UAV equipped with a

multispectral and thermal camera. The method proposed in this work could be improved in the future by adopting a complete UAV SfM + Multispectral + Thermal solution. In this way, the REA from SfM may be used to map water ponding and the multispectral and thermal camera to assess the results, especially regarding the standing water's spatial extent. For example, the relationship between surface temperature and soil moisture (Turner et al., 2011) could be exploited to identify areas potentially subject to ponding.

In general, the assessment of this study's results suggests that the proposed method could map the potential extension and depth of stagnant water in agriculture with reasonable estimation. The role of geomorphology as a key element in water ponding generation and understanding in agricultural landscapes is particularly interesting. For this reason, the research tries to exploit the developments of modern topographic techniques for the identification of critical areas on a large scale. Thanks to the UAV-SfM surveys, the mapping of stagnant water becomes rapid in data acquisition and processing, offering crucial information to stakeholders at low cost. The method, which gains robustness thanks to statistical validation, becomes an attractive tool for preparing agricultural land, identifying areas in subsidence that need reprofiling or ad hoc tillage. Therefore, our research has great applicability in lowland farming and becomes a decision-making utility in designing targeted solutions.

5 | CONCLUSION

Stagnant water in lowland agriculture landscapes represents a threat to crops and cultivation management. In this work, a novel approach is proposed to map the ponding problem using a UAV-SfM technique. This primarily allows us to perform a low-cost analysis compared to other topographic surveying techniques, such as LiDAR. Also, thanks to the rapid data acquisition and processing, the method is also robust at farm scale, proposing an upscale from the experimental plots. Specifically, the morphometric indicator *relative elevation attribute* was used to map the potential water ponding phenomena in such landscapes. The high resolution obtained becomes a key starting point. Indeed, UAV-SfM proved to be very useful for investigating the geomorphic signatures that characterize the agricultural surface. The proposed technique was able to reconstruct in detail even the smallest convexity and concavity of the terrain, offering an interesting insight into the potential occurrence of stagnant water. Furthermore, in this work, an accurate statistical comparison between the results obtained and an in-field campaign of water depth measurement is proposed.

The research outcomes illustrate how a purely morphological approach can be used to identify the potential surface water stagnation phenomena, through expeditious and low-cost topographic surveys using UAV systems.

The results provide useful information for better managing the analysed site, highlighting criticalities related to some non-optimal farming practices. Besides, it could be useful in water stagnation risk prevention and may be used as support for sustainable agricultural management.

ACKNOWLEDGEMENTS

This study was funded by University of Padova research projects DOR1948955/19 'Evaluation of the effectiveness of drainage systems in an agricultural context' and DOR2079232/20 'Soil erosion and waterlogging analysis in agricultural context'. The authors thank Sofia Michieli for providing the study area in which to carry out the research, and helping us in surface water depth data collection. They also thank Xuewei Chen for the support during the GNSS and UAV survey.

CONFLICT OF INTEREST

The authors declare that they have no known competing financial interests or personal relationships that could have appeared to influence the work reported in this paper.

DATA AVAILABILITY STATEMENT

Research data are not shared.

ORCID

Eugenio Straffelini https://orcid.org/0000-0001-5754-7654
Sara Cucchiaro https://orcid.org/0000-0002-8042-836X
Paolo Tarolli https://orcid.org/0000-0003-0043-5226

REFERENCES

Adler, J. & Parmryd, I. (2010) Quantifying colocalization by correlation: The Pearson correlation coefficient is superior to the Mander's overlap coefficient. *Cytometry Part A*, 77(8), 733–742. https://doi.org/10.1002/cyto.a.20896

Appels WM. 2013. Water redistribution at the soil surface: Ponding and surface runoff in flat areas. Available online at: https://edepot.wur.nl/250242 [accessed 8 January 2021].

Archer, N.A.L., Quinton, J.N. & Hess, T.M. (2002) Below-ground relationships of soil texture, roots and hydraulic conductivity in two-phase mosaic vegetation in south-east Spain. *Journal of Arid Environments*, 52(4), 535–553. https://doi.org/10.1006/jare.2002.1011

ARPAV. 2019. Carta dei Suoli del Veneto in scala 1:250.000 – Versione 2019. Available online at: https://www.arpa.veneto.it/temi-ambientali/suolo/conoscenza-dei-suoli/carta-1-250.000/leg_250k.pdf [accessed 8 January 2021].

ARPAV. 2020. Dati meteo-idrologici validati. Available online at: https://www.arpa.veneto.it/dati-ambientali/dati-validati [accessed 8 January 2021].

Bahçeci, İ. & Nacar, A.S. (2009) Subsurface drainage and salt leaching in irrigated land in south-east Turkey. *Irrigation and Drainage: The Journal of the International Commission on Irrigation and Drainage*, 58(3), 346–356. https://doi.org/10.1002/ird.400

Barneveld, R.J., Seeger, M. & Maalen-Johansen, I. (2013) Assessment of terrestrial laser scanning technology for obtaining high-resolution DEMs of soils. *Earth Surface Processes and Landforms*, 38(1), 90–94. https://doi.org/10.1002/esp.3344

Batey, T. (2009) Soil compaction and soil management – a review. *Soil Use and Management*, 25(4), 335–345. https://doi.org/10.1111/j.1475-2743.2009.00236.x

Bendig, J., Bolten, A., Bennertz, S., Broscheit, J., Eichfuss, S. & Bareth, G. (2014) Estimating biomass of barley using crop surface models (CSMs) derived from UAV-based RGB imaging. *Remote Sensing*, 6 (11), 10395–10412. https://doi.org/10.3390/rs61110395

Ben-Hur, M., Yolcu, G., Uysal, H.İ., Lado, M. & Paz, A. (2009) Soil structure changes: Aggregate size and soil texture effects on hydraulic conductivity under different saline and sodic conditions. *Soil Research*, 47(7), 688–696. https://doi.org/10.1071/SR09009

Berli, M., Kulli, B., Attinger, W., Keller, M., Leuenberger, J., Flühler, H., *et al.* (2004) Compaction of agricultural and forest subsoils by tracked heavy construction machinery. *Soil and Tillage Research*, 75(1), 37–52. https://doi.org/10.1016/S0167-1987(03)00160-0

Beven, K.J. & Kirkby, M.J. (1979) A physically based, variable contributing area model of basin hydrology/Un modèle à base physique de

zone d'appel variable de l'hydrologie du bassin versant. *Hydrological Sciences Journal*, 24(1), 43–69. https://doi.org/10.1080/02626667909491834

Bottinelli, N., Hallaire, V., Goutal, N., Bonnaud, P. & Ranger, J. (2014) Impact of heavy traffic on soil macroporosity of two silty forest soils: Initial effect and short-term recovery. *Geoderma*, 217, 10–17. https://doi.org/10.1016/j.geoderma.2013.10.025

Bronswijk, J.J.B. (1991) Drying, cracking and subsidence of a clay soil in a lysimeter. *Soil Science*, 152(2), 92–99.

Carretta L, Tarolli P, Cardinali A, Nasta P, Romano N, Masin R (2021) Evaluation of runoff and soil erosion under conventional tillage and no-till management: A case study in northeast Italy. *Catena*, 197 104972. http://dx.doi.org/10.1016/j.catena.2020.104972

Carrivick, J.L., Smith, M.W. & Quincey, D.J. (2016) , *Structure from motion in the geosciences. New analytical methods in earth and environmental science*. Chichester: John Wiley & Sons, Ltd, https://doi.org/10.1002/9781118895818

Carturan, L., Cazorzi, F. & Dalla Fontana, G. (2009) Enhanced estimation of glacier mass balance in unsampled areas by means of topographic data. *Annals of Glaciology*, 50(50), 37–46. https://doi.org/10.3189/172756409787769519

Cazorzi, F., Fontana, G.D., Luca, A.D., Sofia, G. & Tarolli, P. (2013) Drainage network detection and assessment of network storage capacity in agrarian landscape. *Hydrological Processes*, 27(4), 541–553. https://doi.org/10.1002/hyp.9224

Chang, A., Jung, J., Maeda, M.M. & Landivar, J. (2017) Crop height monitoring with digital imagery from unmanned aerial system (UAS). *Computers and Electronics in Agriculture*, 141, 232–237. https://doi.org/10.1016/j.compag.2017.07.008

Chaplot, V.A. & Le Bissonnais, Y. (2003) Runoff features for interrill erosion at different rainfall intensities, slope lengths, and gradients in an agricultural loessial hillslope. *Soil Science Society of America Journal*, 67(3), 844–851. https://doi.org/10.2136/sssaj2003.8440

Chen, P.H., Leung, K.C. & Wang, J.T. (2000) Investigation of a ponding irrigation system to recycle agricultural wastewater. *Environment International*, 26(1–2), 63–68. https://doi.org/10.1016/S0160-4120(00)00079-9

Chipanshi, A., Fitzmaurice, J., De Jong, R., Bogdan, D., Lewis, M., Kroetsch, D. & Lee, D. (2018) Assessment of soil trafficability across the agricultural region of the Canadian Prairies with the gridded climate data set. *Soil and Tillage Research*, 184, 128–141. https://doi.org/10.1016/j.still.2018.07.003

Cohen, J. (1960) A coefficient of agreement for nominal scales. *Educational and Psychological Measurement*, 20(1), 37–46. https://doi.org/10.1177/001316446002000104

Cox, J.W. & McFarlane, D.J. (1995) The causes of waterlogging in shallow soils and their drainage in southwestern Australia. *Journal of Hydrology*, 167(1–4), 175–194. https://doi.org/10.1016/0022-1694(94)02614-H

Cucchiaro, S., Cavalli, M., Vericat, D., Crema, S., Llena, M., Beinat, A., *et al*. (2018) Monitoring topographic changes through 4D-structure-from-motion photogrammetry: Application to a debris-flow channel. *Environmental Earth Sciences*, 77(18), 632. https://doi.org/10.1007/s12665-018-7817-4

Cucchiaro, S., Fallu, D.J., Zhang, H., Walsh, K., Van Oost, K., Brown, A.G. & Tarolli, P. (2020) Multiplatform-SfM and TLS data fusion for monitoring agricultural terraces in complex topographic and landcover conditions. *Remote Sensing*, 12(12), 1946. https://doi.org/10.3390/rs12121946

Curtis, D.R. & Campopiano, M. (2014) Medieval land reclamation and the creation of new societies: Comparing Holland and the Po Valley, c. 800–c. 1500. *Journal of Historical Geography*, 44, 93–108. https://doi.org/10.1016/j.jhg.2013.10.004

Dong J, Burnham JG, Boots B, Rains G, Dellaert F. 2017. 4D crop monitoring: Spatio-temporal reconstruction for agriculture. In *Proceedings of the 2017 IEEE International Conference on Robotics and Automation (ICRA)*. IEEE: Piscataway, NJ; 3878–3885.

Dunin, F.X. (2002) Integrating agroforestry and perennial pastures to mitigate water logging and secondary salinity. *Agricultural Water Management*, 53(1–3), 259–270. https://doi.org/10.1016/S0378-3774(01)00168-8

Dunn, S.M. & Mackay, R. (1996) Modelling the hydrological impacts of open ditch drainage. *Journal of Hydrology*, 179(1–4), 37–66. https://doi.org/10.1016/0022-1694(95)02871-4

Eisenbeiss, H. & Sauerbier, M. (2011) Investigation of UAV systems and flight modes for photogrammetric applications. *The Photogrammetric Record*, 26(136), 400–421. https://doi.org/10.1111/j.1477-9730.2011.00657.x

Eitel, J.U., Vierling, L.A. & Long, D.S. (2010) Simultaneous measurements of plant structure and chlorophyll content in broadleaf saplings with a terrestrial laser scanner. *Remote Sensing of Environment*, 114(10), 2229–2237. https://doi.org/10.1016/j.rse.2010.04.025

Eltner, A., Kaiser, A., Castillo, C., Rock, G., Neugirg, F. & Abellán, A. (2016) Image-based surface reconstruction in geomorphometry – merits, limits and developments. *Earth Surface Dynamics*, 4(2), 359–389. https://doi.org/10.5194/esurf-4-359-2016

Estornell, J., Ruiz, L.A., Velázquez-Martí, B. & Hermosilla, T. (2011) Analysis of the factors affecting LiDAR DTM accuracy in a steep shrub area. *International Journal of Digital Earth*, 4(6), 521–538. https://doi.org/10.1080/17538947.2010.533201

Frei, S. & Fleckenstein, J.H. (2014) Representing effects of micro-topography on runoff generation and sub-surface flow patterns by using superficial rill/depression storage height variations. *Environmental Modelling & Software*, 52, 5–18. https://doi.org/10.1016/j.envsoft.2013.10.007

Garnero, G. & Godone, D. (2013) Comparisons between different interpolation techniques. *The International Archives of the Photogrammetry, Remote Sensing and Spatial Information Sciences*, 5, W3. https://doi.org/10.5194/isprsarchives-XL-5-W3-139-2013

Gil-Docampo, M.L., Arza-García, M., Ortiz-Sanz, J., Martínez-Rodríguez, S., Marcos-Robles, J.L. & Sánchez-Sastre, L.F. (2020) Above-ground biomass estimation of arable crops using UAV-based SfM photogrammetry. *Geocarto International*, 35(7), 687–699. https://doi.org/10.1080/10106049.2018.1552322

Gonçalves, G.R., Pérez, J.A. & Duarte, J. (2018) Accuracy and effectiveness of low cost UASs and open source photogrammetric software for foredunes mapping. *International Journal of Remote Sensing*, 39(15–16), 5059–5077. https://doi.org/10.1080/01431161.2018.1446568

Grayson, B., Penna, N.T., Mills, J.P. & Grant, D.S. (2018) GPS precise point positioning for UAV photogrammetry. *The Photogrammetric Record*, 33(164), 427–447. https://doi.org/10.1111/phor.12259

Gupta, R.P. (2017) *Remote Sensing Geology*. Berlin: Springer.

Gupta, S.K., Sharma, D.P. & Swarup, A. (2004) Relative tolerance of crops to surface water stagnation. *Journal of Agricultural Engineering*, 41(4), 43–47.

Haghnazari, F., Shahgholi, H. & Feizi, M. (2015) Factors affecting the infiltration of agricultural soils. *International Journal of Agronomy and Agricultural Research*, 6(5), 21–35.

Han, X.F., Jin, J.S., Wang, M.J., Jiang, W., Gao, L. & Xiao, L. (2017) A review of algorithms for filtering the 3D point cloud. *Signal Processing: Image Communication*, 57, 103–112. https://doi.org/10.1016/j.image.2017.05.009

Hobbs, P.R., Sayre, K. & Gupta, R. (2008) The role of conservation agriculture in sustainable agriculture. *Philosophical Transactions of the Royal Society, Series B*, 363(1491), 543–555. https://doi.org/10.1098/rstb.2007.2169

Höhle, J. & Höhle, M. (2009) Accuracy assessment of digital elevation models by means of robust statistical methods. *ISPRS Journal of Photogrammetry and Remote Sensing*, 64(4), 398–406. https://doi.org/10.1016/j.isprsjprs.2009.02.003

Horn, R., Domżżał, H., Słowińska-Jurkiewicz, A. & Van Ouwerkerk, C. (1995) Soil compaction processes and their effects on the structure of arable soils and the environment. *Soil and Tillage Research*, 35(1–2), 23–36. https://doi.org/10.1016/0167-1987(95)00479-C

James, M.R., Robson, S., d'Oleire-Oltmanns, S. & Niethammer, U. (2017) Optimising UAV topographic surveys processed with structure-from-motion: Ground control quality, quantity and bundle adjustment.

Geomorphology, 280, 51–66. https://doi.org/10.1016/j.geomorph.2016.11.021

Javernick, L., Brasington, J. & Caruso, B. (2014) Modeling the topography of shallow braided rivers using structure-from-motion photogrammetry. *Geomorphology*, 213, 166–182. https://doi.org/10.1016/j.geomorph.2014.01.006

Jay, S., Rabatel, G., Hadoux, X., Moura, D. & Gorretta, N. (2015) In-field crop row phenotyping from 3D modeling performed using structure from motion. *Computers and Electronics in Agriculture*, 110, 70–77. https://doi.org/10.1016/j.compag.2014.09.021

Jensen, J. & Mathews, A. (2016) Assessment of image-based point cloud products to generate a bare earth surface and estimate canopy heights in a woodland ecosystem. *Remote Sensing*, 8(1), 50. https://doi.org/10.3390/rs8010050

Kamphorst, E.C. & Duval, Y. (2001) Validation of a numerical method to quantify depression storage by direct measurements on moulded surfaces. *Catena*, 43(1), 1–14. https://doi.org/10.1016/S0341-8162(00)00123-5

Keller, T., Sandin, M., Colombi, T., Horn, R. & Or, D. (2019) Historical increase in agricultural machinery weights enhanced soil stress levels and adversely affected soil functioning. *Soil and Tillage Research*, 194, 104293. https://doi.org/10.1016/j.still.2019.10429

Ladefoged, T.N., McCoy, M.D., Asner, G.P., Kirch, P.V., Puleston, C.O., Chadwick, O.A. & Vitousek, P.M. (2011) Agricultural potential and actualized development in Hawai'i: An airborne LiDAR survey of the leeward Kohala field system (Hawai'i Island). *Journal of Archaeological Science*, 38(12), 3605–3619. https://doi.org/10.1016/j.jas.2011.08.031

Lapena, D.R. & Martz, L.W. (1996) An investigation of the spatial association between snow depth and topography in a prairie agricultural landscape using digital terrain analysis. *Journal of Hydrology*, 184(3–4), 277–298. https://doi.org/10.1016/0022-1694(95)02975-3

Lin, L.I.K. (1989) A concordance correlation coefficient to evaluate reproducibility. *Biometrics*, 45(1), 255–268. https://doi.org/10.2307/2532051

Liu, W., Huang, J., Wei, C., Wang, X., Mansaray, L.R., Han, J., *et al.* (2018) Mapping water-logging damage on winter wheat at parcel level using high spatial resolution satellite data. *ISPRS Journal of Photogrammetry and Remote Sensing*, 142, 243–256. https://doi.org/10.1016/j.isprsjprs.2018.05.024

Mandal, A.K. & Sharma, R.C. (2001) Mapping of waterlogged areas and salt affected soils in the IGNP command area. *Journal of the Indian Society of Remote Sensing*, 29(4), 229–235. https://doi.org/10.1007/BF02995728

Martinez-Agirre, A., Álvarez-Mozos, J., Milenković, M., Pfeifer, N., Giménez, R., Valle, J.M. & Rodríguez, Á. (2020) Evaluation of terrestrial laser scanner and structure from motion photogrammetry techniques for quantifying soil surface roughness parameters over agricultural soils. *Earth Surface Processes and Landforms*, 45(3), 605–621. https://doi.org/10.1002/esp.4758

McCoy, M.D., Asner, G.P. & Graves, M.W. (2011) Airborne lidar survey of irrigated agricultural landscapes: An application of the slope contrast method. *Journal of Archaeological Science*, 38(9), 2141–2154. https://doi.org/10.1016/j.jas.2011.02.033

McFarlane, D.J. & Williamson, D.R. (2002) An overview of water logging and salinity in southwestern Australia as related to the 'Ucarro' experimental catchment. *Agricultural Water Management*, 53(1–3), 5–29. https://doi.org/10.1016/S0378-3774(01)00153-6

Meinen, B.U. & Robinson, D.T. (2020) Mapping erosion and deposition in an agricultural landscape: Optimization of UAV image acquisition schemes for SfM-MVS. *Remote Sensing of Environment*, 239, 111666. https://doi.org/10.1016/j.rse.2020.111666

Merot, P., Ezzahar, B., Walter, C. & Aurousseau, P. (1995) Mapping waterlogging of soils using digital terrain models. *Hydrological Processes*, 9(1), 27–34. https://doi.org/10.1002/hyp.3360090104

Milenković, M., Pfeifer, N. & Glira, P. (2015) Applying terrestrial laser scanning for soil surface roughness assessment. *Remote Sensing*, 7(2), 2007–2045. https://doi.org/10.3390/rs70202007

Mueller, L., Behrendt, A., Schalitz, G. & Schindler, U. (2005) Above ground biomass and water use efficiency of crops at shallow water tables in a temperate climate. *Agricultural Water Management*, 75(2), 117–136. http://doi.org/10.1016/j.agwat.2004.12.006

Neumann, K.J. (2008) Trends for digital aerial mapping cameras. *The International Archives of the Photogrammetry, Remote Sensing and Spatial Information Sciences*, 28, 551–554.

Nguyen, T.T., Slaughter, D.C., Townsley, B., Carriedo, L., Julin, N.N. & Sinha, N. (2016) Comparison of structure-from-motion and stereo vision techniques for full in-field 3D reconstruction and phenotyping of plants: An investigation in sunflower. In: *Proceedings of the 2016 ASABE Annual International Meeting*. St. Joseph, MI: American Society of Agricultural and Biological Engineers Available online at: https://doi.org/10.13031/aim.20162444593

Nunes, M.R., Denardin, J.E., Pauletto, E.A., Faganello, A. & Pinto, L.F.S. (2015) Mitigation of clayey soil compaction managed under no-tillage. *Soil and Tillage Research*, 148, 119–126. https://doi.org/10.1016/j.still.2014.12.007

Pandey, A.C., Singh, S.K. & Nathawat, M.S. (2012) Analysing the impact of anthropogenic activities on waterlogging dynamics in Indo-Gangetic plains, Northern Bihar, India. *International Journal of Remote Sensing*, 33(1), 135–149. https://doi.org/10.1080/01431161.2011.584916

Pásztor, L., Körösparti, J., Bozán, C., Laborczi, A. & Takács, K. (2015) Spatial risk assessment of hydrological extremities: Inland excess water hazard, Szabolcs-Szatmár-Bereg County, Hungary. *Journal of Maps*, 11(4), 636–644. https://doi.org/10.1080/17445647.2014.954647

Pijl, A., Barneveld, P., Mauri, L., Borsato, E., Grigolato, S. & Tarolli, P. (2019a) Impact of mechanisation on soil loss in terraced vineyard landscapes. *Cuadernos de Investigación Geográfica*, 45(1), 287–308. https://doi.org/10.18172/cig.3774

Pijl A, Tosoni M, Roder G, Sofia G, Tarolli P (2019b) Design of Terrace Drainage Networks Using UAV-Based High-Resolution Topographic Data. *Water*, 11 (4), 814. http://dx.doi.org/10.3390/w11040814

Pirotti, F. & Tarolli, P. (2010) Suitability of LiDAR point density and derived landform curvature maps for channel network extraction. *Hydrological Processes: An International Journal*, 24(9), 1187–1197. https://doi.org/10.1002/hyp.7582

Pontius, R.G., Jr. & Millones, M. (2011) Death to kappa: Birth of quantity disagreement and allocation disagreement for accuracy assessment. *International Journal of Remote Sensing*, 32(15), 4407–4429. https://doi.org/10.1080/01431161.2011.552923

Prosdocimi, M., Calligaro, S., Sofia, G., Dalla Fontana, G. & Tarolli, P. (2015) Bank erosion in agricultural drainage networks: New challenges from structure-from-motion photogrammetry for post-event analysis. *Earth Surface Processes and Landforms*, 40(14), 1891–1906. https://doi.org/10.1002/esp.3767

Qureshi, A.S., McCornick, P.G., Qadir, M. & Aslam, Z. (2008) Managing salinity and waterlogging in the Indus Basin of Pakistan. *Agricultural Water Management*, 95(1), 1–10. https://doi.org/10.1016/j.agwat.2007.09.014

R Core Team. 2000. *R: A language and environment for statistical computing*. Available online at: https://www.r-project.org/ [accessed 13 April 2020].

Remondino, F., Nocerino, E., Toschi, I. & Menna, F. (2017) A critical review of automated photogrammetric processing of large datasets. *The International Archives of the Photogrammetry, Remote Sensing and Spatial Information Sciences*, 42, W5. https://doi.org/10.5194/isprs-archives-XLII-2-W5-591-2017

Ritzema, H.P., Satyanarayana, T.V., Raman, S. & Boonstra, J. (2008) Subsurface drainage to combat waterlogging and salinity in irrigated lands in India: Lessons learned in farmers' fields. *Agricultural Water Management*, 95(3), 179–189. https://doi.org/10.1016/j.agwat.2007.09.012

Saadat, S., Frankenberger, J., Bowling, L. & Ale, S. (2020) Evaluation of surface ponding and runoff generation in a seasonally frozen drained agricultural field. *Journal of Hydrology*, 588, 124985. https://doi.org/10.1016/j.jhydrol.2020.124985

Salvucci, G.D. & Entekhabi, D. (1995) Ponded infiltration into soils bounded by a water table. *Water Resources Research*, 31(11), 2751–2759. https://doi.org/10.1029/95WR01954

Saxton, K.E., Rawls, W., Romberger, J.S. & Papendick, R.I. (1986) Estimating generalized soil-water characteristics from texture. *Soil Science*

Society of America Journal, 50(4), 1031–1036. https://doi.org/10.2136/sssaj1986.03615995005000040039x

Servadio, P., Marsili, A., Pagliai, M., Pellegrini, S. & Vignozzi, N. (2001) Effects on some clay soil qualities following the passage of rubber-tracked and wheeled tractors in central Italy. *Soil and Tillage Research*, 61(3–4), 143–155. https://doi.org/10.1016/S0167-1987(01)00195-7

Shore, M., Murphy, P.N.C., Jordan, P., Mellander, P.E., Kelly-Quinn, M., Cushen, M., *et al*. (2013) Evaluation of a surface hydrological connectivity index in agricultural catchments. *Environmental Modelling & Software*, 47, 7–15. https://doi.org/10.1016/j.envsoft.2013.04.003

Sibson, R. (1981) A brief description of natural neighbor interpolation. In: Barnett, V. (Ed.) *Interpreting Multivariate Data*. New York: Wiley, pp. 21–36.

Singh, A. (2015) Soil salinization and waterlogging: A threat to environment and agricultural sustainability. *Ecological Indicators*, 57, 128–130. https://doi.org/10.1016/j.ecolind.2015.04.027

Singh, A. (2017) Waterlogging and salinity management for sustainable irrigated agriculture. II: Engineering measures and biodrainage. *Journal of Irrigation and Drainage Engineering*, 143(9), 04017036. https://doi.org/10.1061/(ASCE)IR.1943-4774.0001227

Snapir, B., Hobbs, S. & Waine, T.W. (2014) Roughness measurements over an agricultural soil surface with structure from motion. *ISPRS Journal of Photogrammetry and Remote Sensing*, 96, 210–223. https://doi.org/10.1016/j.isprsjprs.2014.07.010

Soane, B.D. & Van Ouwerkerk, C. (1994) Soil compaction problems in world agriculture. *Developments in Agricultural Engineering*, 11, 1–21. http://www.sciencedirect.com/science/article/pii/B978044488286850009X, https://doi.org/10.1016/B978-0-444-88286-8.50009-X

Sofia, G., Prosdocimi, M., Dalla Fontana, G. & Tarolli, P. (2014) Modification of artificial drainage networks during the past half-century: Evidence and effects in a reclamation area in the Veneto floodplain (Italy). *Anthropocene*, 6, 48–62. https://doi.org/10.1016/j.ancene.2014.06.005

Stehman, S. (1996) Estimating the kappa coefficient and its variance under stratified random sampling. *Photogrammetric Engineering and Remote Sensing*, 62(4), 401–407.

Suzuki, L.E., Reichert, J.M. & Reinert, D.J. (2013) Degree of compactness, soil physical properties and yield of soybean in six soils under no-tillage. *Soil Research*, 51(4), 311–321. https://doi.org/10.1071/SR12306

Tarolli, P., Cavalli, M. & Masin, R. (2019) High-resolution morphologic characterization of conservation agriculture. *Catena*, 172, 846–856. https://doi.org/10.1016/j.catena.2018.08.026

Tarolli, P., Sofia, G. & Dalla Fontana, G. (2012) Geomorphic features extraction from high-resolution topography: Landslide crowns and bank erosion. *Natural Hazards*, 61(1), 65–83. https://doi.org/10.1007/s11069-010-9695-2

Turner D, Lucieer A, Watson C. 2011. Development of an unmanned aerial vehicle (UAV) for hyper resolution vineyard mapping based on visible, multispectral, and thermal imagery. In *Proceedings of the 34th International Symposium on Remote Sensing of Environment*.

Ullah, W. & Dickinson, W.T. (1979) Quantitative description of depression storage using a digital surface model: I. Determination of depression storage. *Journal of Hydrology*, 42(1–2), 63–75. https://doi.org/10.1016/0022-1694(79)90006-4

Vinci, A., Todisco, F., Brigante, R., Mannocchi, F. & Radicioni, F. (2017) A smartphone camera for the structure from motion reconstruction for measuring soil surface variations and soil loss due to erosion. *Hydrology Research*, 48(3), 673–685. https://doi.org/10.2166/nh.2017.075

Wickham H. 2016. *ggplot2: Elegant graphics for data analysis*. Available online at: https://ggplot2.tidyverse.org [Accessed 13 April 2020].

Xue, Y., Li, Y., Guang, J., Zhang, X. & Guo, J. (2008) Small satellite remote sensing and applications – history, current and future. *International Journal of Remote Sensing*, 29(15), 4339–4372. https://doi.org/10.1080/01431160801914945

Yaalon, D.H. & Kalmar, D. (1984) Extent and dynamics of cracking in a heavy clay soil with xeric moisture regime. In: Bouma, J. & Raats, P.A. C. (Eds.) *Proceedings of the ISSS Symposium on Water and Solute Movement in Heavy Clay Soils*. Wageningen: ILRI, pp. 45–48.

How to cite this article: Straffelini E, Cucchiaro S, Tarolli P. Mapping potential surface ponding in agriculture using UAV-SfM. *Earth Surf. Process. Landforms*. 2021;46:1926–1940. https://doi.org/10.1002/esp.5135